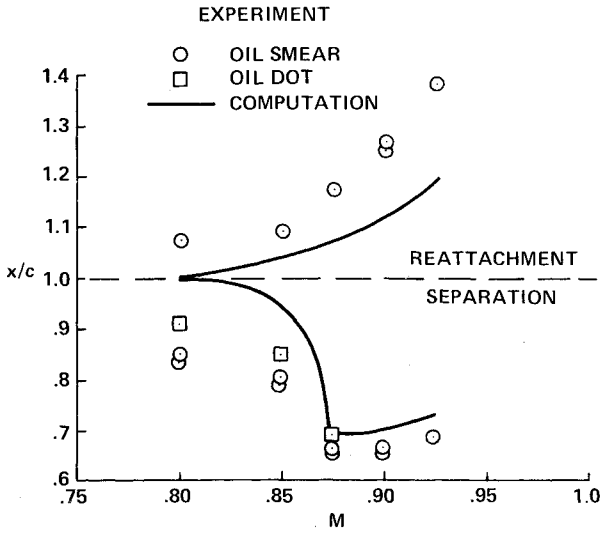

Fig. 3 Comparison of measured and computed separation zones.

conditions probably contributes to a general underprediction of the extent of separation for all subsequent higher Mach numbers. As the Mach number increases to 0.875 where shock-wave-induced separation is present, the computed separation locations are in good agreement with experiment. However, the experimental reattachment location is always significantly downstream of the computed values.

The turbulence model comparisons for the $M=0.875$ and 0.90 cases show that the curvature correction is not important, but the differences between the two-equation and algebraic models are. The algebraic model predicts a shock-wave location significantly downstream of the two-equation result but the shape of the pressure plateau is not too different. This is because the reattachment point for both models is nearly the same and the displacement thicknesses at $x/c=1$ only differ by 10%.

Conclusion

New data have been presented for a transonic shock-wave/boundary-layer interaction flow with separation for a range of freestream Mach numbers. Computed results using a two-equation eddy viscosity turbulence model showed reasonable agreement with the measured pressure distribution at the lower Mach numbers, but as the Mach number increased and the separated zone began to dominate the flowfield, the computations could not accurately predict the flowfield. For all Mach numbers, the length of separated zone was substantially underpredicted. Computed results using an algebraic turbulence model clearly showed these results to be inferior to the two-equation model computations.

References

[1] Johnson, D. A., Horstman, C. C., and Bachalo, W. D., "Comparison Between Experiment and Prediction for a Transonic Turbulent Separated Flow," *AIAA Journal,* Vol. 20, June 1982, pp. 737-744.

[2] Cebecci, T. and Smith, A. M. O., *Analysis of Turbulent Boundary Layers,* Academic Press, New York, 1974.

[3] Jones, W. P. and Launder, B. E., "The Prediction of Laminarization with a Two-Equation Model of Turbulence," *International Journal of Heat and Transfer,* Vol. 15, Feb. 1972, pp. 301-314.

[4] Kline, S. J., Cantwell, B. J.., and Lilley, G. M., eds., "The 1980-81 AFSOR/-HTTM-Stanford Conference on Complex Turbulent Flows: Comparison of Computation and Experiment," Vol. III, Stanford Univ., Stanford, Calif., 1982, pp. 1326-1336.

[5] MacCormack, R.W., "A Numerical Method for Solving the Equations of CompressibleViscous Flow," *AIAA Journal,* Vol. 20, Sept. 1982, pp. 1275-1281.

Nozzle Flow Using the Galerkin Finite Element Method

T. Doan* and R. D. Archer†
The University of New South Wales
New South Wales, Australia

Nomenclature

A	= cross-sectional area; or two-dimensional domain of solution
ℓ	= coordinate index; =0 Cartesian or =1 cylindrical coordinates
L_k, N_i	= shape functions
$\dot{m}$	= mass flow rate
n	= number of nodal points
p	= pressure
r,z	= radial and axial directions (Fig. 1)
R_*	= throat radius of curvature (Fig. 1)
S	= element boundary
t,n	= unit vectors tangential and normal to the surface
u,w,V	= radial, axial, and total velocity
γ	= specific heat ratio, =1.4
ρ	= fluid density
ω	= density correction factor[4]
∇	= divergence operator

Subscripts

i,j,k	= node number
in	= inlet, face AB (Fig. 1)
0	= stagnation condition

Introduction

THE Galerkin technique has opened up the application of the finite element method (FEM)[1] to fluid flow.[2] Consider the well-known problem[3] of steady, inviscid, compressible perfect gas flow in an arbitrarily shaped, axisymmetric nozzle. Many recent FEM solutions[4-6] to fluid flow problems have adopted the velocity potential (ϕ), or stream function (ψ), as dependent variables in the governing equations. Reference 7 simplifies the differential equations in each element by a local linearization process; Ref. 8 used groups of (primitive) variables, namely (ρu, ρw, ρuw), giving a system of nonlinear equations; and Ref. 9 employs a least-squares criterion on a system of two first-order equations, continuity and irrotationality, written in terms of (ρ,u,w).

Here, we report the results of the Galerkin FEM applied with linear shape functions to the equations of motion, Eqs. (1-4), in the primitive variables (ρ,u,w), combined with the irrotationality condition, Eq. (5).

Basic Equations and Assumptions

The nozzle (Fig. 1) is made up of a constant diameter inlet length and simple convergent-divergent cones, interconnected by sections whose wall shapes are circular arcs. In cylindrical (r,z) coordinates, the governing equations under steady-state conditions are as follows.

Received March 23, 1983; revision received Aug. 8, 1983.

*Graduate Student; currently, Engineer, Generation and Operations Department, Queensland Electricity Generation Board, Brisbane.

†Associate Professor, School of Mechanical and Industrial Engineering.

Continuity

$$\nabla \cdot \rho V r^{\ell} = \frac{\partial}{\partial r}(\rho u r^{\ell}) + \frac{\partial}{\partial z}(\rho w r^{\ell}) = 0 \tag{1}$$

Euler

$$\rho(V\cdot\nabla)V = -\nabla p, \text{ i.e.} \begin{cases} \frac{1}{\rho}\frac{\partial p}{\partial z} + w\frac{\partial w}{\partial z} + u\frac{\partial w}{\partial r} = 0 & (2) \\ \frac{1}{\rho}\frac{\partial p}{\partial r} + u\frac{\partial u}{\partial r} + w\frac{\partial u}{\partial z} = 0 & (3) \end{cases}$$

Entropy

$$p = \rho^{\gamma}(p_0/\rho_0^{\gamma}) \tag{4}$$

Assuming irrotationality, no shock waves or boundary-layer effects

$$\nabla \times V = 0, \text{ i.e., } \frac{\partial u}{\partial z} - \frac{\partial w}{\partial r} = 0 \tag{5}$$

Refer velocities to $V_{\max} = \sqrt{(2/(\gamma-1))\cdot(p_0/\rho_0)}$; p and ρ to stagnation p_0 and ρ_0; and lengths to the radius at the geometric throat. Combining Eqs. (2-5)

$$\rho = (1 - u^2 - w^2)^{1/\gamma - 1} \tag{6}$$

Because, when introduced to Eqs. (1), (5), and (6), the Galerkin criterion generates nonlinear equations in ρ, u, and w, the density ρ will be prescribed to render equations linear and easily solved for u, w. Iteration on ρ achieves convergence.

Chain differentiate Eq. (1) to give

$$\rho r^{\ell}\frac{\partial u}{\partial r} + \rho u \ell r^{\ell-1} + u r^{\ell}\frac{\partial \rho}{\partial r} + \rho r^{\ell}\frac{\partial w}{\partial z} + w r^{\ell}\frac{\partial \rho}{\partial z} = 0 \tag{7}$$

Even though $\rho = 0(V^{2/(\gamma-1)}) = 0(V^5)$ for $\gamma = 1.4$, a lower order interpolation function can be used between nodal densities in an element. Approximate

$$\rho = \sum_k L_k(r,z)\cdot\rho_k \tag{8}$$

$$\begin{bmatrix} u \\ w \end{bmatrix} = \sum_i N_i(r,z)\begin{bmatrix} u_i \\ w_i \end{bmatrix} \tag{9}$$

Substitute Eqs. (8) and (9) into Eqs. (5) and (7) for the following residuals:

$$R_1 = \sum_i u_i\left[\frac{\partial N_i}{\partial r} r^{\ell}\sum_k L_k\rho_k + \ell r^{\ell-1} N_i \sum_k L_k\rho_k + r^{\ell} N_i \sum_k \frac{\partial L_k}{\partial r}\rho_k\right] + \sum_i w_i\left[\frac{\partial N_i}{\partial z} r^{\ell}\sum_k L_k\rho_k + r^{\ell} N_i \sum_k \frac{\partial L_k}{\partial z}\cdot\rho_k\right] \tag{10}$$

$$R_2 = \sum_i u_i\frac{\partial N_i}{\partial z} - \sum_i w_i\frac{\partial N_i}{\partial r} \tag{11}$$

With nodal ρ's known before each iteration, apply the Galerkin criterion to Eqs. (10) and (11), and then Green's theorem to Eq. (12).

$$\iint_A N_j R_1 \mathrm{d}r\mathrm{d}z = 0, \quad \iint_A N_j R_2 \mathrm{d}r\mathrm{d}z = 0 \qquad j = 1,n \tag{12}$$

$$\sum_{i=1}^{n} a_{ji}u_i + \sum_{i=1}^{n} b_{ji}w_i = 0, \quad \sum_{i=1}^{n} c_{ji}u_i + \sum_{i=1}^{n} d_{ji}w_i = 0 \qquad j = 1,\ldots,n \tag{13}$$

where

$$a_{ji} = \sum_k \rho_k \int_S r^{\ell} N_i N_j L_k \mathrm{d}z - \sum_k \rho_k \int_A r^{\ell} N_i L_k \frac{\partial N_j}{\partial r}\mathrm{d}r\mathrm{d}z$$

$$b_{ji} = \sum_k \rho_k \int_S r^{\ell} N_i N_j L_k \mathrm{d}r - \sum_k \rho_k \int_A r^{\ell} N_i L_k \frac{\partial N_j}{\partial z}\mathrm{d}r\mathrm{d}z$$

$$c_{ji} = \int_S N_i N_j \mathrm{d}r - \int_A N_i \frac{\partial N_j}{\partial z}\mathrm{d}r\mathrm{d}z$$

$$d_{ji} = -\int_S N_i N_j \mathrm{d}z + \int_A N_i \frac{\partial N_j}{\partial r}\mathrm{d}r\mathrm{d}z$$

Solve Eq. (13) for u_i and w_i. Nodal density can then be updated using Eq. (6).

$$\rho_i^{(n+1)} = \rho_i^{(n)} + \omega[(1 - u_i^2 - w_i^2)^{1/(\gamma-1)} - \rho_i^{(n)}] \tag{14}$$

Convergence can be accelerated by an appropriate choice of $\omega \sim 1.4$.

Boundary Conditions

The precursor disturbance caused by the inlet contraction curvature, $R_{\text{in}} = 1.5$, vanishes well within a length $L = 6$ of the duct, upstream of which the flow is uniform, face AB (Fig. 1). Thus, $u_{\text{in}} = 0$; $w_{\text{in}} = \text{const} = (\dot{m}/\rho_{\text{in}} A_{\text{in}})$. Impermeability at the wall and symmetry at the centerline require $V\cdot n = 0$; and take outlet face CD (Fig. 1) as part of a spherical potential surface of a conical source flow $V\cdot t = 0$.

Table 1 Computing time

Mesh	I	II	III	IV
Relative time/iteration	1	6	45	200
Iterations				
Case 1	9	9	9	5[a]
Case 2	—	25	25	9[a]

[a] Starting from converged solution for mesh III.

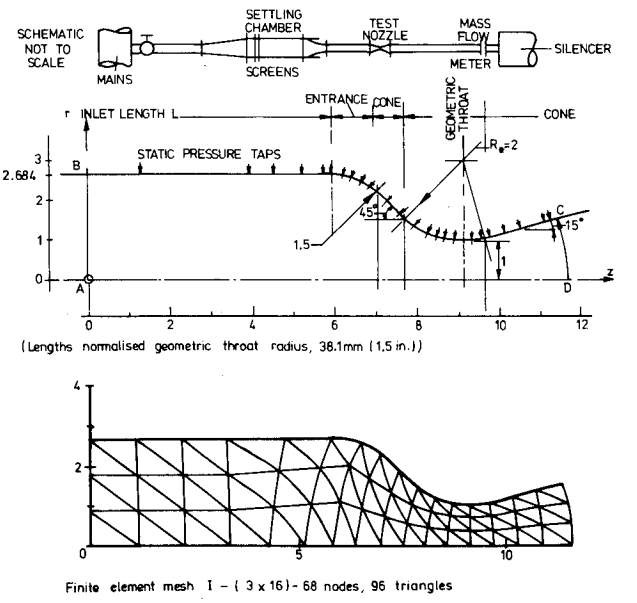

Fig. 1 Nozzle geometry and mesh.

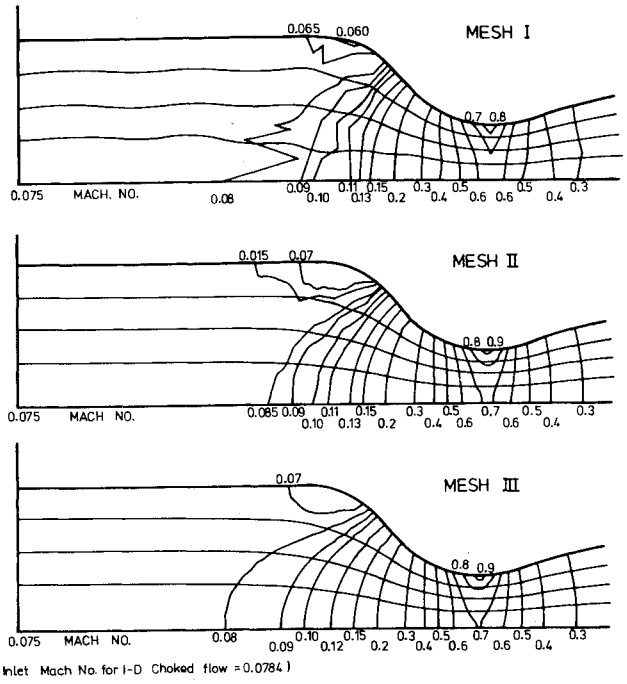

Fig. 2a Predicted compressible flowfield: −96% of one-dimensional mass flow.

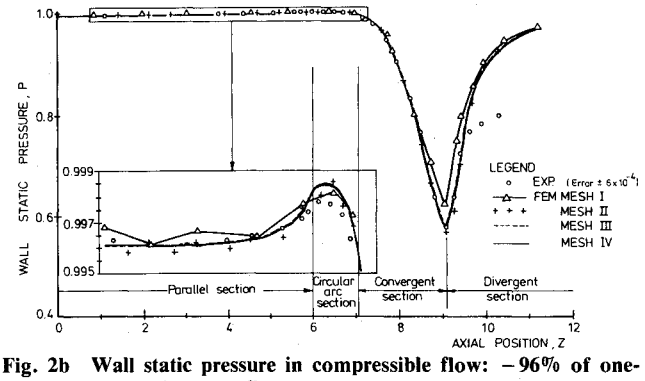

Fig. 2b Wall static pressure in compressible flow: −96% of one-dimensional choking mass flow.

Results and Discussion

Figure 2 gives computed results for the nozzle defined in Fig. 1. Four successively refined triangular element meshes were generated. Meshes II, III, and IV have element sizes 1/2, 1/4, and 1/6 of those of mesh I. The elementary one-dimensional solution value of ρ was used to start the iteration process. Linear interpolation functions were used to approximate ρ, u, and w.

The choked mass flow rate for this nozzle ($R_* = 2.0$) is ~99.4% of the one-dimensional choking mass flow.[10] Two cases of near choking flow are reported: 1) 96% of the one-dimensional choking mass flow and 2) flow with a small supersonic pocket, 99.3% of one-dimensional choking flow, the highest achieved. Table 1 gives computing times.

Experiments on the nozzle of Fig. 1 used ambient air compressed to 446 kPaa (65 psia) and dried to −45°C (−50°F) dew point. Wall static pressure taps, Fig. 1, were 0.8-mm (0.032-in.) diameter. A liquid manometer was used for small pressure differences in the inlet contraction and approach duct, and a Druck pressure transducer accurate to 1 in 3500 elsewhere. Mass flow rates accurate to ±1% were measured using a VDI nozzle of 40.47-mm (1.60-in.) diameter. Inlet flow Reynolds number was 8×10 based on pipe diameter.

Figure 2b compares computed and experimental wall-pressure distributions for case 1. The FEM predicts the extent of the region of adverse pressure gradient in the inlet section.

Meshes II-IV gave smooth velocity contours and streamlines for case 2, which contains a supersonic pocket, with a maximum wall Mach number of 1.13. The slower convergency of this case is consistent with the fact that the Galerkin criterion is basically an elliptic operator. The method was successfully applied to a nozzle with $R_* = 0.625$.

References

[1] Zienkiewicz, O. C., *The Finite Element Method in Engineering Science*, 2nd ed., McGraw Hill, London, 1971.

[2] Fletcher, C.A.J., "The Galerkin Method: An Introduction," *Numerical Simulation of Fluid Motion*, edited by J. Noye, North Holland, Amsterdam, 1978.

[3] Midgal, D., Klein, K., and Moretti, G., "Time-Dependent Calculations for Transonic Nozzle Flow," *AIAA Journal*, Vol. 7, Feb. 1969, pp. 372-374.

[4] Labujere, Th.E. and Van der Vooren, J., "Finite Element Calculations of Axisymmetric Subcritical Compressible Flow," NLR-TR 74162 U, 1974.

[5] Periaux, J., "3-D Analysis of Compressible Potential Flows with the Finite Element Method," *International Journal for Numerical Methods in Engineering*, Vol. 9, No. 4, 1975, pp. 775-832.

[6] Chan, S.T.K., Brashears, M. R., and Young, V.C.Y., "Finite Element Analysis of Transonic Flow by Method of Weighted Residuals," AIAA Paper 75-79, 1975.

[7] Shen, S. F. and Habashi, W., "Local Linearization of the Finite Element Method and its Application to Compressible Flow," *International Journal for Numerical Methods in Engineering*, Vol. 10, May-June 1976, pp. 565-577.

[8] Fletcher, C.A.J., "The Primitive Variables Finite Element Formulation for Inviscid Compressible Flow," *Journal of Computational Physics*, Vol. 33, Dec. 1979, pp. 301-312.

[9] Chattot, J. J., Guiu-Roux, J., and Laminie, J., "Finite Element Calculation of Steady State Transonic Flow in Nozzles using Primary Variables," *Lecture Notes in Physics*, Vol. 141, Springer-Verlag, Berlin, 1981, pp. 107-112..

[10] Back, L. H., Massier, P. F., and Gier, H. L., "Comparison of Measured and Predicted Flows through Conical Supersonic Nozzles with Emphasis on the Transonic Region," *AIAA Journal*, Vol. 3, Sept. 1965, pp. 1606-1614.

Frozen-Plasma Boundary-Layer Flows over Adiabatic Flat Plates

G. Ben-Dor,* Z. Rakib,† and O. Igra‡
Ben-Gurion University of the Negev, Beer Sheva, Israel

Introduction

THE nonlinear partial differential equations describing most boundary-layer problems are difficult to solve. Consequently, many investigators resort to using simplifying similarity transformations. In complex flows, where similarity solutions cannot be used, an exact solution for the general boundary-layer flow equations is not possible. Reviews of commonly used techniques for solution of boundary-layer problems can be found in Refs. 1-3.

One type of boundary-layer problem is the shock wave generated boundary layer. For strong shock waves, the shock-induced flow must be considered as real gas, i.e., plasma. The ionized gas can be in a nonequilibrium, equilibrium, or frozen

Received Aug. 18, 1983.

*Senior Lecturer, Department of Mechanical Engineering.
†Ph.D. Student, Department of Mechanical Engineering.
‡Associate Professor, Department of Mechanical Engineering.